JGR Atmospheres

RESEARCH ARTICLE
10.1029/2022JD037718

Key Points:

- The soil moisture estimates assimilated by Soil Moisture Active Passive onto the offline land surface model were initialized in the Weather Research and Forecasting model
- Advanced soil moisture initialization represented the observed land–atmosphere interaction in the 2016 Northeast Asia heat wave

Supporting Information:

Supporting Information may be found in the online version of this article.

Correspondence to:

D.-H. Cha and C.-K. Song,
dhcha@unist.ac.kr;
cksong@unist.ac.kr

Citation:

Yoon, D., Kang, T., Cha, D.-H., Song, C.-K., Lee, M.-I., Min, K.-H., et al. (2023). Role of land–atmosphere interaction in the 2016 Northeast Asia heat wave: Impact of soil moisture initialization. *Journal of Geophysical Research: Atmospheres*, *128*, e2022JD037718. https://doi.org/10.1029/2022JD037718

Received 31 AUG 2022
Accepted 23 DEC 2022

Author Contributions:

Conceptualization: Donghyuck Yoon, Dong-Hyun Cha, Chang-Keun Song, Myong-In Lee, Ki-Hong Min, Joowan Kim, Eunkyo Seo
Data curation: Donghyuck Yoon, Eunkyo Seo
Investigation: Donghyuck Yoon, Taehun Kang
Methodology: Donghyuck Yoon, Dong-Hyun Cha, Chang-Keun Song, Myong-In Lee, Ki-Hong Min, Joowan Kim, Jong Ahn Chun, Eunkyo Seo
Project Administration: Myong-In Lee
Software: Jong Ahn Chun
Supervision: Dong-Hyun Cha, Chang-Keun Song
Validation: Donghyuck Yoon
Visualization: Donghyuck Yoon
Writing – original draft: Donghyuck Yoon, Taehun Kang, Dong-Hyun Cha

Role of Land–Atmosphere Interaction in the 2016 Northeast Asia Heat Wave: Impact of Soil Moisture Initialization

Donghyuck Yoon[1], Taehun Kang[1], Dong-Hyun Cha[1], Chang-Keun Song[1], Myong-In Lee[1], Ki-Hong Min[2], Joowan Kim[3], Jong Ahn Chun[4], and Eunkyo Seo[5]

[1]Department of Urban and Environmental Engineering, Ulsan National Institute of Science and Technology, Ulsan, Republic of Korea, [2]Department of Astronomy and Atmospheric Sciences, Kyungpook National University, Daegu, Republic of Korea, [3]Department of Atmospheric Science, Kongju National University, Gongju, Republic of Korea, [4]Prediction Research Department, APEC Climate Center, Busan, Republic of Korea, [5]Department of Environmental Atmospheric Sciences, Pukyong National University, Busan, Republic of Korea

Abstract The impact of soil moisture initialization on the 2016 Northeast Asian heat wave was explored using the Land Information System (LIS) Weather Research and Forecasting (WRF) model. To obtain advanced soil moisture estimates, various meteorological variables from the Global Data Assimilation System analysis and Integrated Multi-Satellite Retrievals for Global Precipitation Measurement observation data were used as atmospheric forcings for the offline simulation of the Noah land surface model (Noah-LSM). Based on the LIS, Soil Moisture Active Passive satellite were assimilated in the Noah LSM simulation. The assimilated soil moisture estimates revealed the drier land surface conditions over Northeast Asia compared with the product from the National Centers for Environmental Prediction Final Analysis (FNL) and were used as the initial condition of the WRF model. The WRF experiment initialized by the assimilated soil moisture product (LIS experiment) exhibited the observed surface air temperature (SAT) and 500 hPa geopotential height (500 GPH) over Northeast Asia compared with the result from the experiment initialized by the FNL (CTL experiment). At Week 1, the LIS experiment simulated warmer SAT than that from the CTL experiment, which was induced by the negative anomaly of latent heat flux over Mongolia. Then, 500 GPH became strong and spatially expanded in response to the thermal low induced by the warmer SAT, and the SAT was further increased during Weeks 2 and 3.

Plain Language Summary The association between soil moisture and land–atmosphere interaction occurring in the East Asia were analyzed by focusing on the 2016 extreme heat wave case. The numerical experiment with the initial soil moisture from the fusion of satellite data and land surface model output simulated a more realistic land–atmosphere interaction over East Asia within a 3-week heat wave simulation period, compared to the experiment with the operational soil moisture product.

1. Introduction

The recent increase in severe heat waves is a crucial indicator of global warming and has caused considerable socioeconomic damage (Azhar et al., 2014; Coumou et al., 2013; Knowlton et al., 2009; Meehl & Tebaldi, 2004; Poumadere et al., 2005). Recently, East Asia has experienced record-breaking heat waves, such as those in 2016 and 2018 (Deng et al., 2019; Min et al., 2020; Ren et al., 2020; Yeh et al., 2018; Yoon et al., 2021). According to the Korean Meteorological Administration and the Korea Centers for Disease Control and Prevention, 2,125 and 4,526 cases of heat-related diseases were reported in 2016 and 2018 in South Korea due to extreme heat wave for 22 and 31 days, respectively (Yoon et al., 2021). Li et al. (2022) reported that a record-breaking marine heat wave over the Yellow Sea occurred in August 2016, which was the warmest month ever recorded since 1982. In addition, the China Meteorological Administration issued heat wave alerts for 33 days in 2018. In Japan, at least 1,032 people died from heat-related illnesses in July 2018 (Imada et al., 2019).

Extreme heat waves and high surface air temperature (SAT) can be affected by the soil moisture conditions of the region. Particularly, a lack of soil moisture could promote the increase in SAT under heat wave conditions (Fischer et al., 2007; Lorenz et al., 2010; Miralles et al., 2012, 2014; Seo et al., 2019, 2020; Yoon et al., 2018). Yoon et al. (2018) suggested that lower initial soil moisture content (SMC) during the 2015 South Korean heat wave resulted in reduced evaporation from the land to the atmosphere. They revealed that the surface heat fluxes

Writing – review & editing: Donghyuck Yoon, Taehun Kang, Dong-Hyun Cha, Chang-Keun Song, Myong-In Lee, Ki-Hong Min, Joowan Kim, Jong Ahn Chun, Eunkyo Seo

(i.e., latent and sensible heat fluxes) are strongly associated with the soil moisture conditions during heat wave periods and that the increase in surface flux induced by drier soil conditions could significantly enhance the heat waves. In addition to surface fluxes, various studies have emphasized the importance of the land–atmosphere feedback process due to dry soil moisture anomalies (Dirmeyer et al., 2021; Fischer et al., 2007; Martius et al., 2021; Miralles et al., 2019; Schumacher et al., 2022; Seneviratne et al., 2010; Seo & Dirmeyer, 2022; Zhang & Frederiksen, 2003). Fischer et al. (2007) reported that dry soil conditions not only constrained surface latent heat flux (LHF) but also intensified heat wave by maintaining anticyclonic circulation in response to soil moisture-induced low-level heat in the 2003 European heat wave. Similarly, Miralles et al. (2019) found that there were teleconnected land–atmosphere feedbacks during the 2010 Russian heat wave by self-propagating anticyclones under dry soil conditions.

The potential risk of compound droughts and heat waves is increasing over northern China and Mongolia with recent dry soil conditions and the resulting land–atmosphere feedback (Erdenebat & Sato, 2016, 2018; Y.-W. Seo et al., 2021; Wei et al., 2021; Zhang et al., 2020). Zhang et al. (2020) reported that the frequency of compound drought and heat wave events has been rapidly increasing over inner Northeast Asia, including Mongolia and northern China. They revealed that heat waves associated with dry soil conditions were promoted by anticyclonic anomalies, resulting from land–atmosphere interactions. Wei et al. (2021) revealed the interaction between land and atmosphere over northern China by elucidating the association among SAT, surface sensible heat flux, surface pressure, cloud, precipitation, and soil moisture (see Figure 7 of Wei et al., 2021). In particular, Erdenebat and Sato (2018) showed that the association between the land–atmosphere feedback and SAT over Northeast Eurasia varied spatiotemporally during the 2002 heat wave event by comparing the data of numerical experiments with and without soil moisture–atmosphere interaction. However, there are only a few modeling studies on the relationship between land and atmosphere interactions and heat wave events over Northeast Asia regarding predictions at short-to medium-range time scales.

The soil moisture is a key variable in improving the extended-range forecast due to its persistence (Dirmeyer et al., 2016). and Seo and Dirmeyer (2022) addressed the soil moisture memory in the timely filtered satellite-based product is up to ∼15 days over Northeast Asia. Several studies have introduced the importance of the initial soil moisture conditions of numerical weather prediction models during Northeast Asian heat waves (Wang et al., 2019; Zeng et al., 2014). Zeng et al. (2014) showed that heat wave events with drought could be magnified, as the initial soil moisture conditions more strongly affected diabatic processes (e.g., surface fluxes) than adiabatic processes (e.g., subsidence) at a short-range time scale (∼24 hr). Wang et al. (2019) also carried out numerical experiments and demonstrated that decreased initial soil moisture enhanced extremely high-temperature events over eastern China in 2003, 2007, and 2013. They revealed that reductions in the initial soil moisture conditions force anticyclonic (cyclonic) anomalies in the mid(low)-level of the troposphere. This change can increase the atmosphere thickness, which can expand the anomalous anticyclone that is favorable for severe heat wave events. However, both studies had limitations in that the initial soil moisture conditions were simply controlled by linear multiplication (forcing increase or decrease of initial soil moisture), that is, realistic initial soil moisture condition was not reflected. Therefore, modeling experiments with realistic soil moisture initialization are warranted, which can improve not only the simulation performance but also the reliability of the land–atmosphere interaction exploration for extreme temperature events (Koster & Suarez, 2003; T. S. Lin & Cheng, 2016; Prodhomme et al., 2016; Quesada et al., 2012; Seneviratne et al., 2006; Seo et al., 2019, 2020; van den Hurk et al., 2012). For example, Seo et al. (2019) improved model predictions in SAT for the 2003 and 2010 heat wave events in Europe and Russia by employing a realistic initial soil moisture condition and suggested that prescribing realistic soil moisture conditions at the start of the model simulation is crucial for maintaining anticyclonic circulation anomalies associated with both heat wave events. The 2016 Eurasian heat wave, characterized by much higher than normal temperatures over eastern Europe, East Asia, and the Kamchatka Peninsula, was also related to the strong land–atmosphere coupling attributed to the heterogeneous dry conditions across the Eurasia continent (Seo et al., 2020).

Offline simulation of the land surface model (LSM) by forcing meteorological reanalysis and observational data is widely used to produce realistic initial soil moisture conditions (Chen et al., 2007; Chun et al., 2020; Lim, Byun, et al., 2012; Rodell et al., 2004; Santanello et al., 2016; Xia et al., 2012). It has the advantage of generating high-resolution, homogeneous initial soil moisture conditions using forcing data (observation or analysis field) and parameter data. However, due to insufficient observational data and the uncertainty of reanalysis forcing, soil moisture products from offline LSM can have errors. To overcome this limitation, the soil moisture data

assimilation technique is used to combine remote sensing observations with LSM simulations. Many studies have proven that soil moisture assimilation using both satellite observations and model simulations produces more accurate soil moisture estimations than those obtained using models or observations alone (Draper et al., 2012; Jun et al., 2021; Kumar et al., 2008; P. Lin et al., 2016, 2020; Reichle et al., 2008; Santanello et al., 2016; E. Seo et al., 2021).

In this study, we examine how soil moisture initialization affects the land–atmosphere interaction during the 2016 Northeast Asia heat wave using different soil moisture products as the initial lower-boundary conditions of a numerical weather prediction model. First, a soil moisture initialization system is established by adopting the Land Information System (LIS) and the Weather Research and Forecast (WRF) model. Then, the impacts of soil moisture initialization are evaluated and compared to in-situ observation data and reanalysis meteorological fields. Finally, we investigate the spatiotemporal characteristics of land–atmosphere interactions during the 2016 heat wave over Northeast Asia. The data and methods are described in Section 2. The detailed analysis is presented in Section 3. Section 4 contains the summary and discussion.

2. Data and Method

2.1. Establishing Soil Moisture Initialization System

2.1.1. Offline Land Surface Modeling

We apply the National Aeronautics and Space Administration (NASA) LIS framework for offline land surface modeling and soil moisture data assimilation. Land Information System software allows to accurately simulate land surface conditions by integrating satellite and in-situ data along with various LSMs (Kumar et al., 2006). To obtain realistic and homogeneous gridded soil moisture conditions, offline land surface modeling is performed using Noah LSM version 3.3. Noah LSM divides the ground into four depth layers (0–10, 10–30, 30–60, and 60–100 cm) to simulate various parameters including soil moisture, soil temperature, snow thickness, energy, and water flux, which are calculated based on water and energy budget equations within the LSM (Chen et al., 1996; Koren et al., 1999).

To reproduce realistic land conditions, the analysis product from the National Center for Environmental Prediction (NCEP) Global Data Assimilation System (GDAS) data by the Global Land Data Assimilation System team (National Climatic Data Center; https://portal.nccs.nasa.gov/lisdata_pub/data/MET_FORCING/) is used as a forcing variable of the LSM. For example, SAT, specific humidity, shortwave and longwave radiations, and horizontal wind are used as the forcing variables from GDAS data. As precipitation is the most dominant factor influencing soil moisture in the LSM (E. Seo et al., 2021), Integrated Multi-Satellite Retrievals for Global Precipitation Measurement (IMERG) data (Huffman, Bolvin, Braithwaite, et al., 2015; Huffman, Bolvin, Nelkin, et al., 2015) are also used in addition to the GDAS data for precipitation forcing. The horizontal resolution of the LSM is 0.125° within the Northeast Asian region, and the forcing datasets (i.e., GDAS and IMERG) with approximately 0.1° horizontal resolution are linearly interpolated to the spatial resolution of the model. The offline simulation is conducted starting on 1 January 2016 for 1 year, until 1 January 2017. Spin-ups ranging from a few years to decades are essential for producing an equilibrated soil condition at the time of model initialization (Cosgrove et al., 2003; Lim, Hong, & Lee, 2012; Rodell et al., 2005). Therefore, the offline LSM simulation is run repeatedly until the soil moisture reaches equilibrium, as in the study of Jun et al. (2021). In addition, the soil moisture retrieval from the ninth consecutive run is used to create ensemble spreads in the data assimilation step.

2.1.2. Soil Moisture Data Assimilation

To obtain more accurate soil moisture conditions, satellite soil moisture retrievals are assimilated during the offline LSM simulation. The L-band (1.4 GHz) Soil Moisture Active and Passive (SMAP) Level 3 product (O'Neill et al., 2021) is employed for the purpose. Hu et al. (2022) reported that SMAP soil moisture had a greater accuracy with in-situ stations in inner Mongolia than the soil moisture products from Soil Moisture and Ocean Salinity data; moreover, SMAP near-surface retrieval has been used extensively in recent land data assimilation studies (Lu et al., 2017; Reichle et al., 2017; E. Seo et al., 2021; Tangdamrongsub et al., 2020). Soil moisture retrievals from the SMAP satellite are assimilated using an ensemble Kalman filter (EnKF) algorithm. The EnKF in the LIS framework has been widely employed to assimilated soil moisture retrievals (Kumar et al., 2012, 2019; Reichle et al., 2002, 2008; Santanello et al., 2016).

Table 1
Parameters for Generating Perturbations

Perturbation variable	Additive (A)/ multiplicative (M)	Standard deviation	AR1 time correlation (h)	Cross-correlation						
				SW	LW	PR	SMC1	SMC2	SMC3	SMC4
SW	M	0.2	24	1.0	−0.3	−0.5				
LW	A	30	24	−0.3	1.0	0.5				
PR	M	0.5	24	−0.5	0.5	1.0				
SMC1	A	0.06	3				1.0	0.6	0.4	0.2
SMC2	A	0.011	3				0.6	1.0	0.6	0.4
SMC3	A	0.006	3				0.4	0.6	1.0	0.6
SMC4	A	0.004	3				0.2	0.4	0.6	1.0

Note. SW is downward shortwave radiation, LW is downward longwave radiation, PR is precipitation, and SMC1–SMC4 are the LSM prognostic soil moisture from the first to the fourth soil layer.

As soil moisture retrievals and land model products can be biased due to the uncertainties of forcing data and LSM physics, observational biases are corrected before assimilation using the cumulative distribution function matching method (Jun et al., 2021; Reichle & Koster, 2004; E. Seo et al., 2021). Selected meteorological forcing and model output variables are perturbed using a statistical method following Jun et al. (2021) and E. Seo et al. (2021) (Table 1). Descriptions of the perturbations for the surface forcing and land model variables are further provided in the model and data section of E. Seo et al. (2021).

2.2. Numerical Experiments

The WRF version 3.9.1 (Skamarock et al., 2005) is employed for the numerical model simulation of the atmosphere. Our WRF model domain includes Mongolia (42.5°–50°N, 95°–115°E; blue shading in Figure 1a) and Northeast Asia (34°–50°N, 95°–131°E; red dashed line in Figure 1a) with a 12-km horizontal resolution. The simulation is conducted for 2016, beginning at 00 UTC on 16 July 2016, and run for 21 days until 00 UTC on 6 August 2016, when continental thermal highs developed with increasing SAT over Northeast Asia (Figure 1b). Six-hourly NCEP GDAS final analysis (Prediction Final Analysis [FNL]) data in a 0.25° × 0.25° horizontal resolution is used for the initial and lateral boundary conditions of the atmosphere.

The impact of soil moisture initialization on the land–atmosphere interactions during the heat wave is investigated by comparing the WRF model experiments using different initial soil moisture conditions. These initial

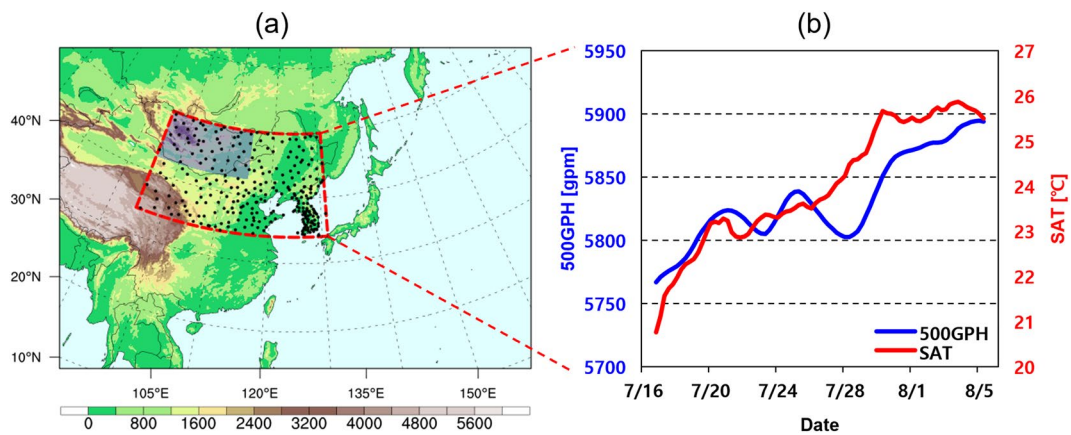

Figure 1. (a) Topographical height (m) in the and Weather Research and Forecast|Weather Research and Forecasting domain with locations of HadISD stations (black dots). Red dashed lines and blue shaded area indicate Northeast Asia (34°–50°N, 95°–131°E) and Mongolia (42.5°–50°N, 95°–115°E) areas, respectively. (b) Time series of 500-hPa geopotential height (500 GPH, unit: gpm) and surface air temperature (°C) over Northeast Asia from HadISD and Prediction Final Analysis data during the simulation period.

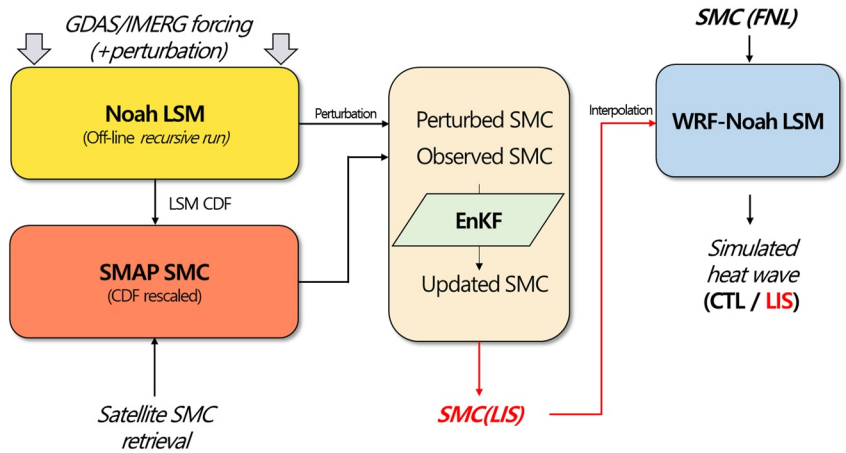

Figure 2. Schematic diagram of the soil moisture initialization system used in this study. SMC, soil moisture content; CDF, cumulative distribution function.

conditions are obtained from the FNL data (CTL experiment) and the LIS soil moisture data assimilation product (LIS experiment), respectively. For physical parameterizations, single-moment six-class microphysics scheme (Hong & Lim, 2006), New Simplified Arakawa–Schubert parameterization scheme (Han & Pan, 2011), and Yonsei University planetary boundary layer scheme (Hong et al., 2006) are employed. For longwave and shortwave radiation parameterizations, the rapid radiative transfer model scheme (Dudhia, 1989) is used. The FNL and the ERA5 reanalysis data are also used to evaluate the synoptic fields from the simulated results. The higher-resolution model results (i.e., WRF model result in 12-km grid resolution) are converted to the FNL analysis grid using bilinear interpolation. Hourly SAT data from the Hadley Centre Integrated Surface Database (HadISD; Dunn et al., 2016) are also employed for evaluating the simulated SATs. The simulated SATs are bilinearly interpolated to the location of the station. Figure 2 shows the schematic flow of the entire soil moisture initialization and the numerical experiment process in this study.

3. Results

3.1. Assessment of the Impact of Soil Moisture Initialization

Through offline land surface modeling with soil moisture data assimilation, the Noah LSM generally simulated drier surface soil conditions than the FNL soil moisture data over the Northeast Asia region at the start of the model simulation (Figure 3). Especially, the LSM simulated dry SMC (~0.2 m^3 m^{-3}) mostly over Mongolia (brown shading in Figure 3). The difference over Northeast Asia at the start of the model simulation was almost maintained throughout the simulation period, which can be considered as the impact of the initial soil moisture condition (Figure 3c). These characteristics (i.e., drier soil over Northeast Asia in the offline LSM spin-up) were also observed in the deeper soil layers (Figure S1 in Supporting Information S1).

Next, atmospheric conditions simulated from the numerical experiments using the WRF model were spatially assessed by comparing to the FNL analysis field and HadISD in-situ station data (Figure 4). During the simulation period, Northeast Asia experienced severe heat waves with an anomalous mid-level anticyclone that covered the region from Mongolia to the Korean Peninsula (Li et al., 2022; Yeh et al., 2018; Yoon et al., 2021). The daily mean observed SAT at several stations in southern Mongolia, eastern China, and South Korea exceeded 28°C (Figure 4a). It is 3°C higher than the climatological mean of SAT over South Korea, based on the data from the Korean Meteorological Administration (https://data.kma.go.kr/resources/html/en/aowdp.html). In contrast, this warming event was not well reproduced in the CTL experiment. In the CTL experiment, negative 500 hPa geopotential height (500 GPH) biases, with the maxima over Mongolia and the Korean Peninsula, prevailed over the anticyclonic region (Figure 4b). SAT was also underestimated by up to 3°C in the same regions, whereas the model overestimated SAT over eastern China (Figure 4b). The mean absolute errors (MAEs) for 500 GPH and SAT over Northeast Asia were 23.23 geopotential meters (gpm) and 1.21°C, respectively. However, the biases considerably decreased through the soil moisture initialization by the LIS spin-up (Figure 4c). The MAEs of

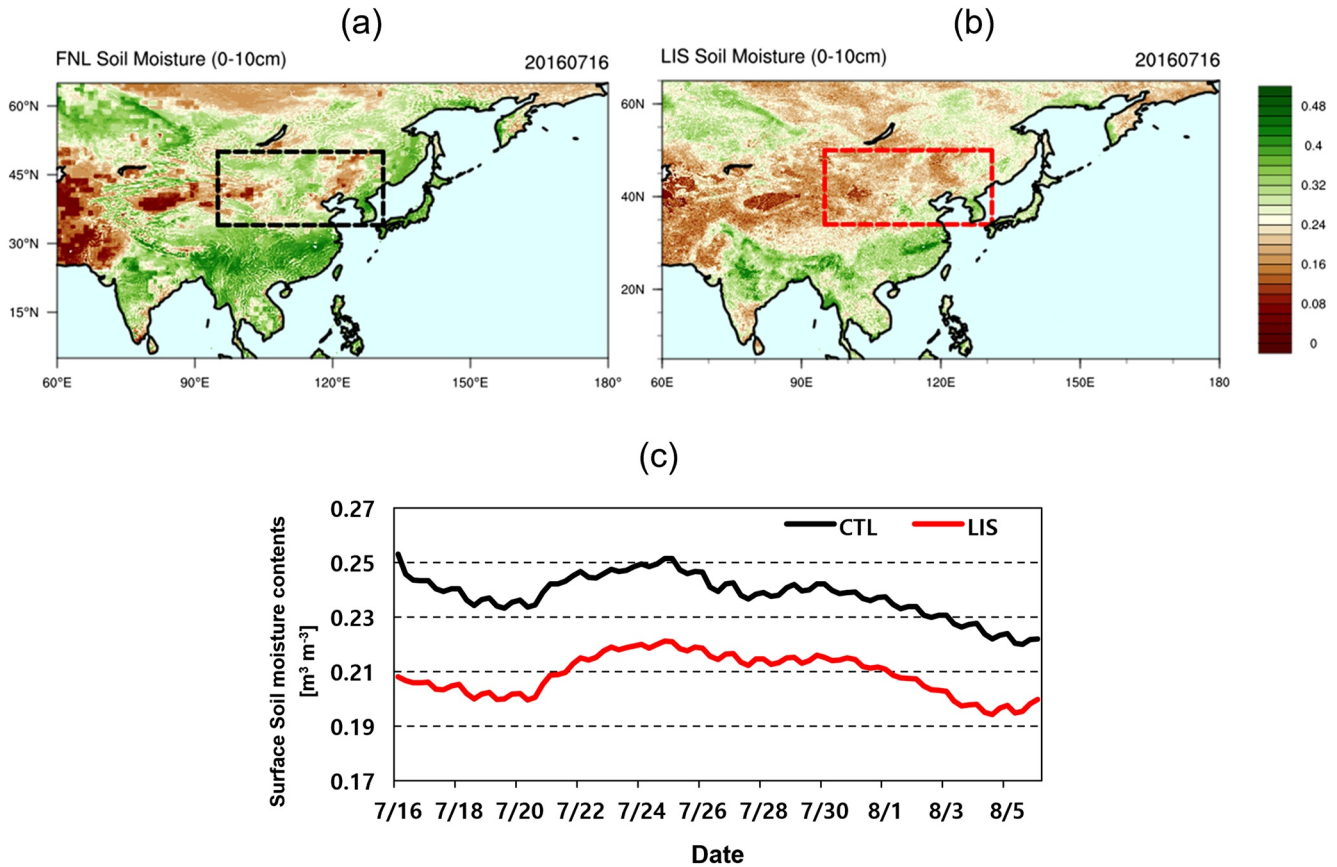

Figure 3. Spatial distribution of surface soil moisture content ($m^3\ m^{-3}$) at 00 UTC on 16 July 2016 simulated in (a) CTL and (b) Land Information System experiments, and (c) their temporal variations over Northeast Asia during the simulation period. Black and red dashed lines in (a) and (b) indicate the Northeast Asia region (34°–50°N, 95°–131°E).

500 GPH and SAT over Northeast Asia in the LIS experiment were 16.68 gpm and 0.65°C, respectively. In particular, the negative biases both in 500 GPH and SAT were remarkably reduced over Mongolia during the simulation period. Note that the validation for 500 GPH using other reanalysis data such as European Centre for Medium-Range Weather Forecasts ERA-5 data (https://rda.ucar.edu/datasets/ds630.0/) did not significantly change the result (Figure S3 in Supporting Information S1).

Temporal variations in the 500 GPH and SAT biases averaged over Northeast Asia were also analyzed (Figure 5). The CTL experiment (with the FNL initial soil moisture) tended to underestimate SAT for the entire simulation period, and the SAT bias became larger when the negative 500 GPH bias was prominent. For example, in the CTL experiment, the SAT bias reached −1.94°C on August 3, with −33.67 gpm 500 GPH bias at that time. These biases in 500 GPH and SAT in the CTL experiment were substantially reduced in the LIS experiment by applying the LIS spin-up for the soil moisture initialization. The SAT bias started to improve from Week 1 (16–23 July), and the improvement was enhanced as the simulation progressed. In particular, the simulation of SAT was most significantly improved in 2 weeks from the initialization (i.e., Week 3; 30 July–6 August), when the 500 GPH bias was substantially reduced.

The MAEs of 500 GPH and SAT and their differences between the CTL and LIS experiments were quantitatively examined (Table 2). Since the impact of soil moisture initialization by LIS spin-up was more notable over Mongolia than over Northeast Asia (Figure 4) and varied through the simulation period (Figure 5), the errors and differences were investigated for both regions and each week separately. In the CTL experiment, the MAEs of 500 GPH and SAT increased as the simulation continued, with maximum values in Week 3 (27.92 gpm and 1.44°C over Northeast Asia, and 34.06 gpm and 4.17°C over Mongolia) when the LIS experiment achieved the largest improvements. For instance, the differences in 500 GPH and SAT MAEs between the CTL and LIS experiments over Northeast Asia (Mongolia) for Week 3 were 19.75 gpm (25.24 gpm) and 0.84°C (3.31°C),

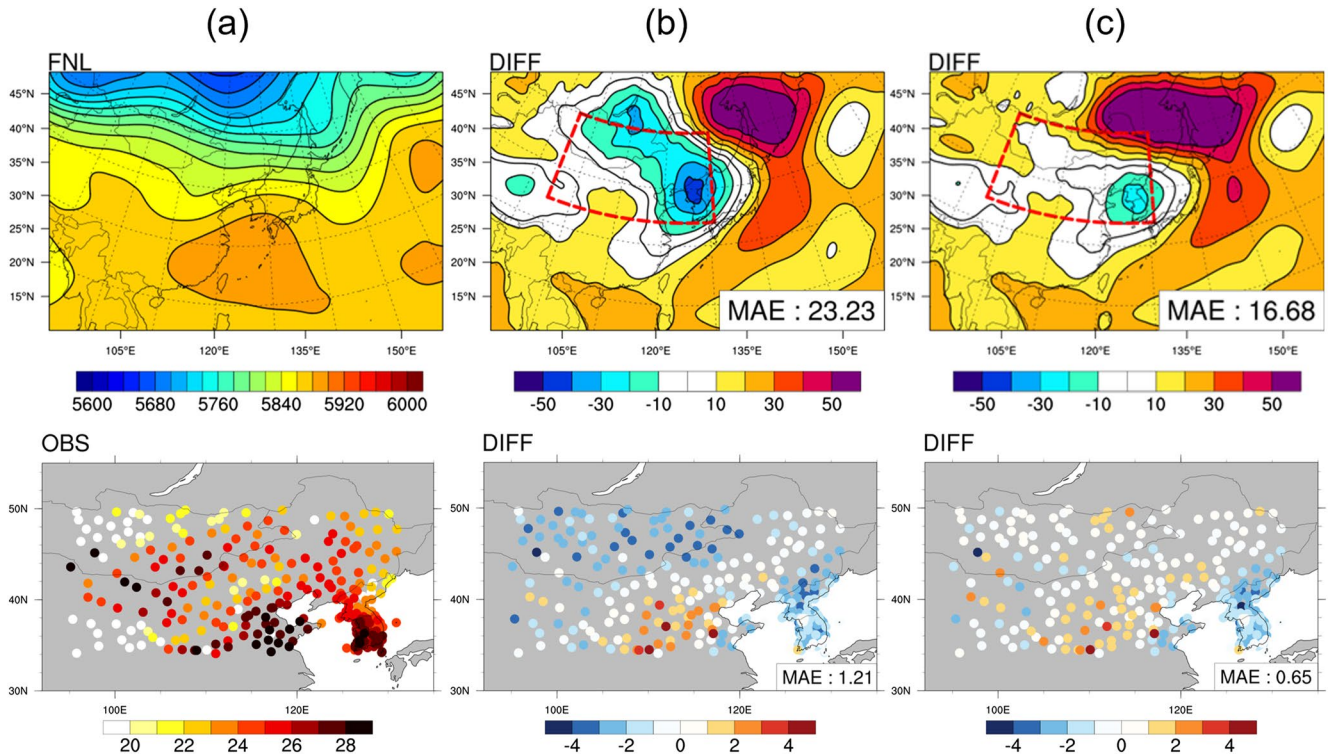

Figure 4. 500 GPH (gpm) (top) and surface air temperature (°C) (bottom) in (a) reanalysis and observation data, and their biases in the (b) CTL experiment and (c) Land Information System experiment during the simulation period. The numbers in the bottom-right boxes in (b) and (c) indicate the area averages of the mean absolute error over Northeast Asia (34°–50°N, 95°–131°E), which are indicated with red dashed lines.

respectively. The spin-up initialization impact also existed from Week 1, especially on the SAT. For example, the MAE of SAT over Mongolia was reduced by 1.04°C in the LIS experiment, although most impacts were negligible in Week 1 (e.g., MAE differences for 500 GPH over Mongolia and for 500 GPH and SAT over Northeast Asia). The SAT improvement was also significant (1.57°C) in Week 2 (23–30 July) over Mongolia. It is noteworthy that the improvement in the 500 GPH biases by applying the LIS spin-up in both weeks (i.e., Weeks 1 and 2) was not significant over Mongolia (0.64 and −2.86 gpm in Weeks 1 and 2, respectively).

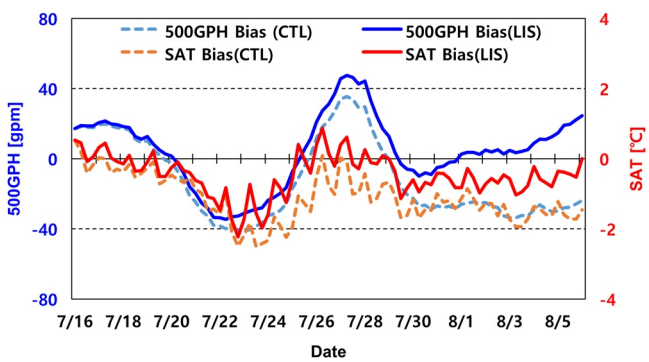

Figure 5. Time series of 6-hourly biases for 500 GPH (gpm) and surface air temperature (°C) over Northeast Asia (34°–50°N, 95°–131°E) during the simulation period.

3.2. Role of Land–Atmosphere Interaction

From the experiment results in the previous section, we found that soil moisture initialization could improve the prediction of 500 GPH and SAT in the 2016 Northeast Asia heat wave event, but the relevant physical processes are not fully understood. Therefore, in this section, we explored the physical mechanisms to explain the spatiotemporal variation in the impacts of soil moisture initialization in detail by focusing on the interaction between SAT and a synoptic field (i.e., mid-level pressure pattern). In the LIS experiment, there was drier surface soil over Northeast Asia throughout the simulation period (Figures 3c and 6a). This spatial pattern of difference in the surface SMC (ΔSM; LIS-CTL) averaged for the simulation period was similar to that at the beginning of the simulation (Figure S2a in Supporting Information S1). The positive SAT difference (ΔSAT; LIS-CTL) in the LIS experiment coincides well with the dry ΔSM throughout the simulation period, particularly over Mongolia and the Tibetan Plateau. It is worth noting that the magnitude of ΔSAT was significantly large (over 3°C; yellow shading in Figure 6b) over Mongolia compared to that over the Tibetan Plateau, and its spatial distribution widely extended to the northeast of Northeast Asia.

Table 2
500 GPH (gpm) and Surface Air Temperature (°C) Mean Absolute Errors (MAEs) in the CTL and Land Information System Experiments With Their Differences

	Northeast Asia						Mongolia					
	500 GPH (gpm)			SAT (°C)			500 GPH (gpm)			SAT (°C)		
	Week 1	Week 2	Week 3	Week 1	Week 2	Week 3	Week 1	Week 2	Week 3	Week 1	Week 2	Week 3
CTL MAE	20.25	22.51	27.92	0.74	1.28	1.44	11.35	13.26	34.06	1.76	2.26	4.17
LIS MAE	18.76	23.24	8.17	0.58	0.63	0.60	10.71	16.12	8.82	0.72	0.69	0.86
LIS-CTL MAE	1.49	−0.73	19.75	0.16	0.65	0.84	0.64	−2.86	25.24	1.04	1.57	3.31

The interactions between 500 GPH and SAT can be clearly seen in the time series of 500 GPH difference (Δ500GPH; LIS-CTL) and ΔSAT averaged over Mongolia (Figure 6c). As mentioned in the previous section, there was a considerable ΔSAT (1–2°C) from the start of the model simulation (Week 1), but Δ500 GPH was considerably smaller than that for the other periods (~10 gpm; see also Table 2). In contrast, ΔSAT substantially increased after 30 Jul, and it is remarkable that Δ500 GPH also increased with ΔSAT, reaching the maximum in Week 3. In other words, it is evident that the land–atmosphere feedback over Mongolia was significantly active during Week 3.

The land-atmosphere interaction described previously is further clarified in Figure 7. In Week 1, Δ500 GPH was negligible, although positive ΔSAT around 1–2°C existed over Mongolia (Figure 7a). Particularly, negative values of LHF difference (ΔLHF; LIS-CTL) and ΔSM (i.e., lower LHF and drier soil in the LIS experiment) prevailed over Mongolia, which had a well-consistent spatial pattern with ΔSAT (Figure 7d). Previous studies

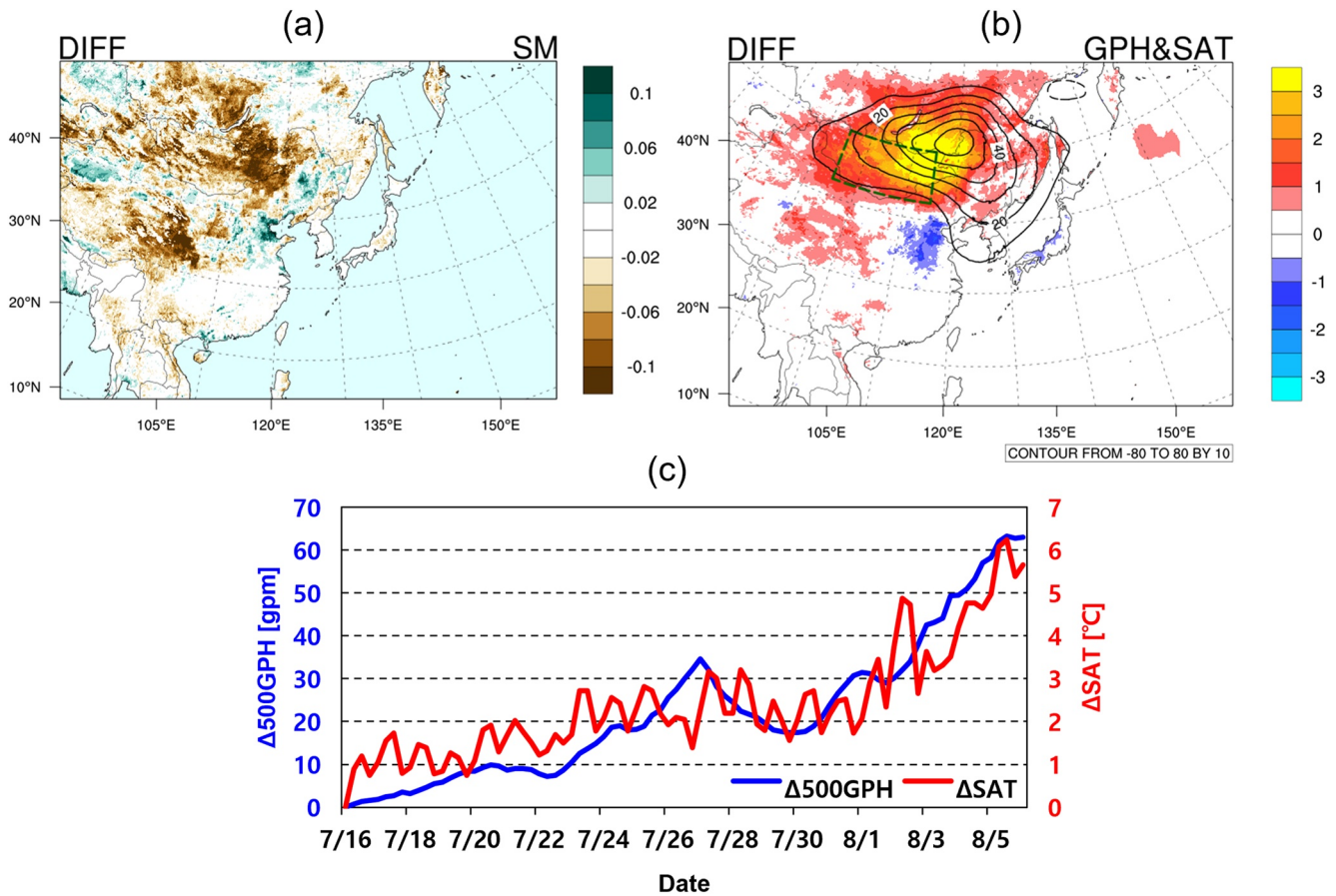

Figure 6. (a) ΔSM ($m^3\ m^{-3}$) and (b) Δ500 GPH (gpm) (contour) with ΔSAT (°C) (shading) during the simulation period. The green dashed lines in (b) indicate the Mongolia area (42.5°–50°N, 95°–115°E). (c) Time series of Δ500°GPH and ΔSAT over Mongolia during the simulation period. Δ indicates differences in variables between the Land Information System and CTL experiment.

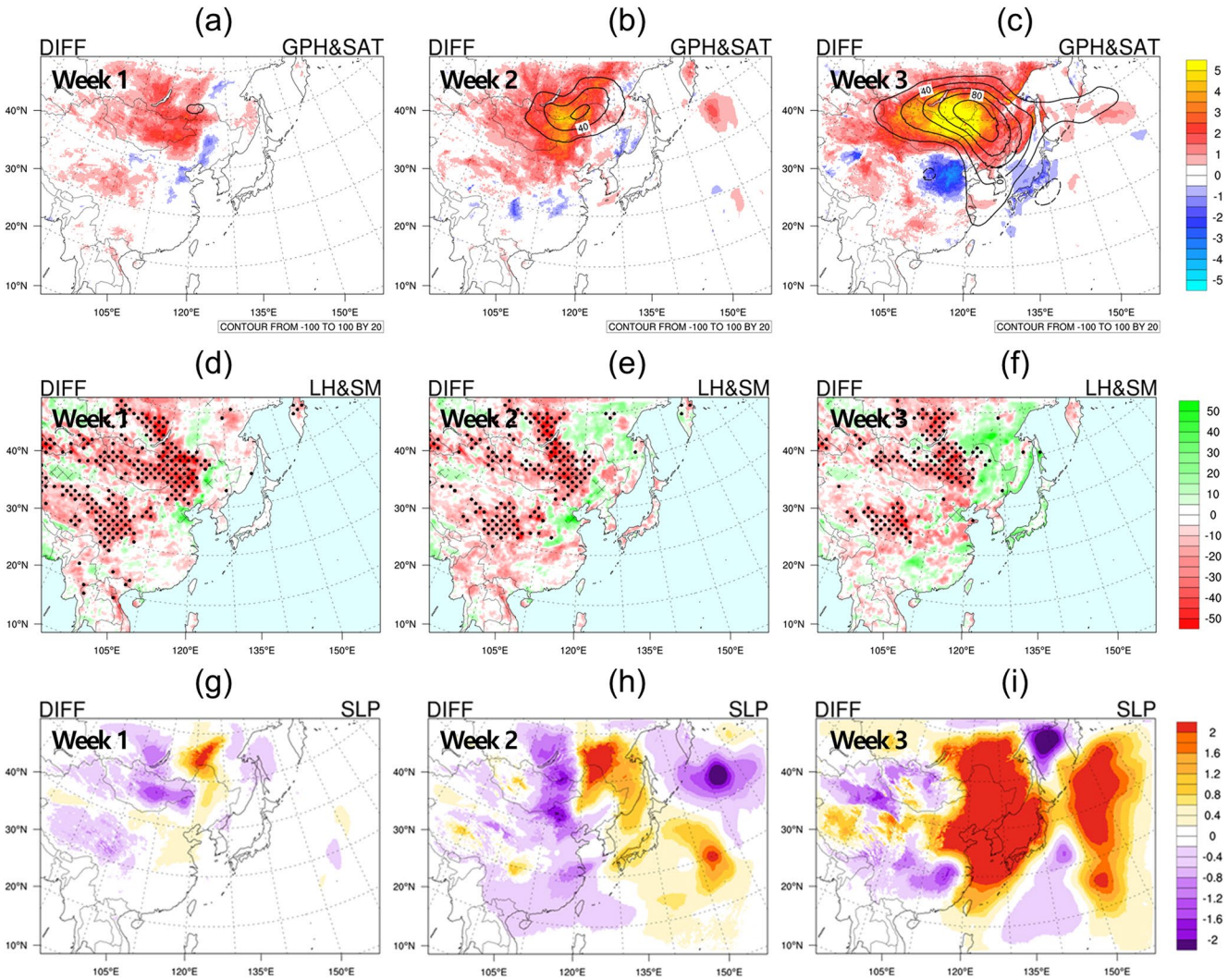

Figure 7. (a–c) Δ500 GPH (gpm) (contour) with ΔSAT (°C) (shading), (d–f) ΔLHF (W m^{-2}) (shading) with ΔSM (m^3 m^{-3}) (>0.05 m^3 m^{-3} is shown in crossed lines and <−0.05 m^3 m^{-3} is shown in dots), and (g–i) ΔSLP (hPa) in (left; a, d, g) Week 1, (mid; b, e, g) Week 2, and (right; c, f, i) Week 3. Δ indicates differences in variables between the Land Information System and CTL experiments.

suggested that a lack of soil moisture can reduce LHF (enhanced sensible heat flux) from the land to the atmosphere and intensify extreme high-temperature events (Fischer et al., 2007; Yoon et al., 2018). Thus, the effect of drier soil on SAT in Week 1 (i.e., increased SAT over Mongolia) was more related to surface conditions such as the reduction in LHF induced by decreasing surface SMC, than the atmospheric conditions such as 500 GPH.

Concurrently, there was a lower sea level pressure (SLP) over Mongolia in the LIS experiment than in the CTL experiment, and that continued until Week 2 (Figures 7g and 7h). It can be considered as strengthening of "thermal low" in response to more dry and hot conditions over Mongolia by LIS spin-up. According to a previous study (Martius et al., 2021), thermal lows can be defined as "areas of low surface pressure that form over warm landmasses with an overlaying mid-tropospheric anticyclone." By developing thermal low over Mongolia, the mid-level anticyclone difference (i.e., Δ500 GPH) was also increased (Figure 7b); correspondingly, the ΔSAT became stronger in Week 2 (Figure 7b), whereas the ΔLHF and ΔSM maintained their spatial distribution and strength similar to those in Week 1 (Figure 7e). Finally, a strong anticyclone anomaly covered Northeast Asia in Week 3, and the largest ΔSAT collocated with the area of the maximum Δ500 GPH and minimum ΔLHF occurred (Figure 7c). Moreover, there are some regions where the spatial patterns of ΔSAT and ΔLHF were inconsistent at that time (Figure 7f), which means that the ΔSAT was mainly responding to the 500 GPH differences in these regions in Week 3. This result indicates the existence of a "non-local impact" of soil moisture

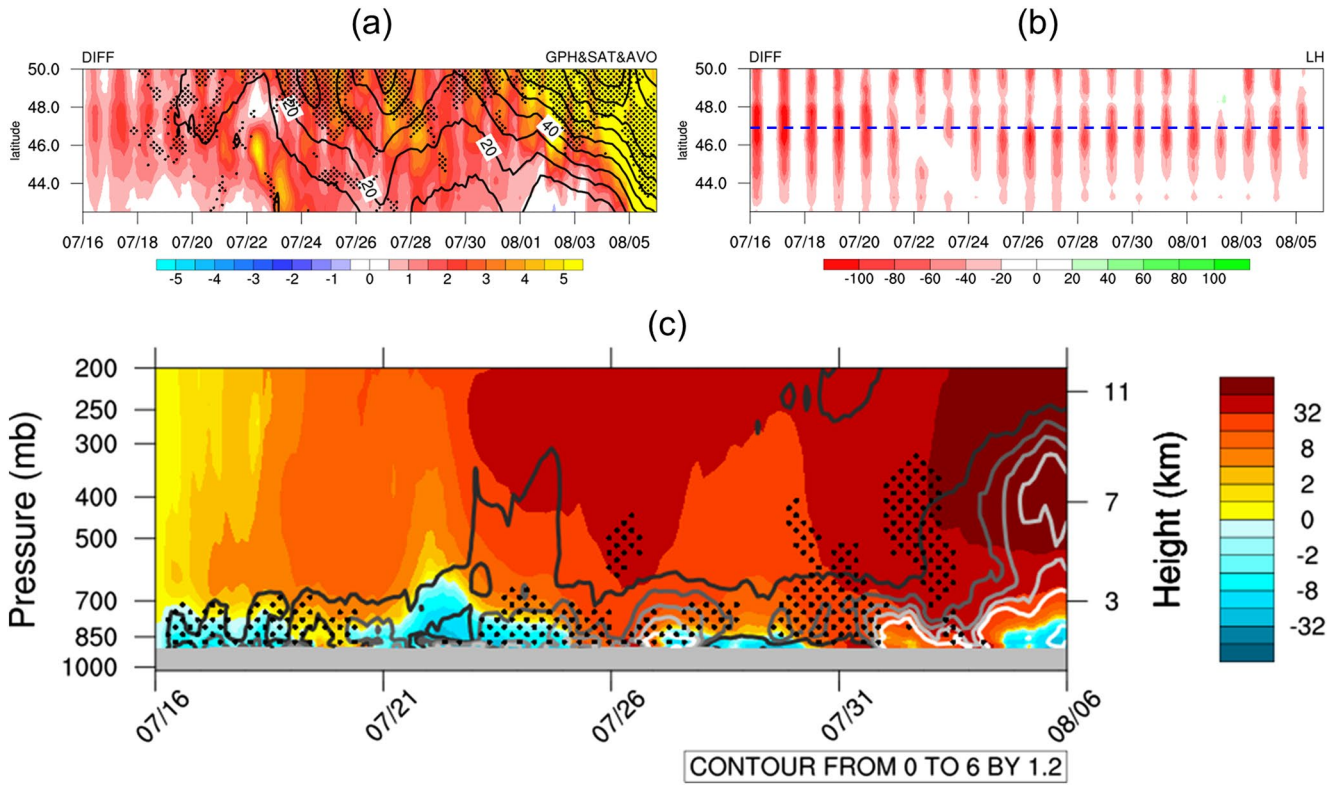

Figure 8. Hovmöller plots of (a) Δ500 GPH (gpm) (contour) and Δ500AVO (s^{-1}) (dots; only $<-1{\cdot}10^{-5}$ s^{-1} is shown) with ΔSAT (°C) (shading) and (b) ΔLHF ($W\ m^{-2}$) averaged over Mongolia (42.5°–50°N, 95°–115°E). Blue dashed line in (b) indicates central Mongolia (47.5°N, 95°–115°E). (c) Vertical structure of ΔGPH (gpm) (shading), ΔT (°C) (contour from 0 to 6 by 1.2 where black contour at 1°C and white contour at 6°C), and ΔQ ($kg^3\ kg^{-3}$) (dots; only $<-0.5{\cdot}10^{-3}\ kg^3\ kg^{-3}$ is shown) averaged over central Mongolia. Δ indicates the differences in variables between the Land Information System and CTL experiments.

initialization (i.e., by affecting large-scale circulation patterns Miralles et al., 2019; Seneviratne et al., 2010; Zhang & Frederiksen, 2003) due to the land–atmosphere feedback over Northeast Asia, and it is consistent with the findings of previous studies that emphasized dry soil-induced land–atmosphere feedback during the heat wave event (Erdenebat & Sato, 2016; Fischer et al., 2007; Miralles et al., 2019; Wei et al., 2021). A positive difference in SLP (ΔSLP; LIS-CTL) also prevailed with the substantial increase in Δ500 GPH (Figure 7i). Accordingly, some areas over Northeast Asia experienced the non-local effect of soil moisture initialization, which manifested as increasing SAT despite the absence of the negative ΔSM.

The mechanism of the land-atmospheric interaction was further examined using Hovmöller and vertical cross-section plots (Figure 8). The Hovmöller plot was determined by zonally averaging the Mongolian region (42.5°–50°N, 95°–115°E; blue shading in Figure 1a). From the beginning of the simulation, the ΔSAT of approximately 1.5°C continued with a diurnal variation, with the maximum value during the day (Figure 8a). However, the variability of ΔSAT decreased during Weeks 2 and 3, and the strength of ΔSAT increased with the increase in Δ500 GPH. Additionally, the variation in ΔSAT was highly similar to the pattern of ΔLHF in Week 1 (Figure 8b), whereas this pattern more correlated with Δ500 GPH and the negative difference in 500 hPa absolute vorticity (Δ500AVO; LIS-CTL) than with ΔLHF in the late period. Previous studies have indicated that the soil moisture initialization effect can be diabatically enhanced during the day when the incoming shortwave radiation is strong (Fischer et al., 2007; Yoon et al., 2018; Zeng et al., 2014); therefore, the results imply that there was a diabatic effect of soil moisture initialization (independent of the mid-atmospheric condition) caused by the changing LHF over Mongolia during Week 1. Consequently, the initialization led to reduced SAT errors over Mongolia in Week 1, as described in Section 3.1 (Table 2). Thereafter, the effect of the land–atmosphere feedback process induced from the soil moisture initialization became more dominant, resulting in larger improvements in both SAT and GPH over Northeast Asia in Week 3 (Table 2). Figure 8c shows the vertical structure of differences in geopotential height (ΔGPH), air temperature (ΔT), and specific

humidity (ΔQ) between the LIS and CTL experiments during the simulation period. All variables were zonally averaged over the area where the soil moisture initialization effect was robust (47.5°N, 95°–115°E; blue dashed line in Figure 8b). In Week 1, there was thermal low with a positive (negative) ΔT (ΔQ) in the lower atmosphere (i.e., 900–700 hPa) due to the drier initial soil condition in the LIS experiment. In particular, the vertical distributions of the low-level positive ΔT, negative ΔGPH, and negative ΔQ were almost consistent during this period. This feature also appeared in the horizontal field (Figures 7a, 7d, and 7g). In contrast, a positive ΔGPH occurred between the mid-to-upper troposphere (700–200 hPa). This can be considered as the response of atmospheric circulation to the low-level heat source induced by dry soil, as described in previous studies (Erdenebat & Sato, 2018; Fischer et al., 2007; Seo et al., 2019; Wei et al., 2021). Although the interaction seems to be activated during the early period of simulation, the interaction strength was too small to make a significant land–atmosphere feedback process or have a non-local effect (Figure 7a). During Weeks 2 and 3, an anticyclonic anomaly in the mid-to-upper atmosphere became significant (Figure 8a), and the ΔT expanded vertically simultaneously. For example, the ΔT of 1°C (black contour in Figure 8c) occurred up to 250 hPa, and the ΔT was over 6°C in the lower atmosphere (white contour in Figure 8c). The heat lows occasionally disappeared from 25 to 27 July and 30 July to 6 August because the positive Δ500 GPH reached the lower atmosphere over Mongolia as the mid-level anticyclonic anomaly moved northeastward (Figures 7c and 7i; Wei et al., 2021).

4. Summary and Discussion

We explored the role of land–atmosphere interaction during the 2016 Northeast Asian heat wave focusing on the impact of soil moisture initialization. Meteorological variables from the GDAS analysis data and IMERG observation data were used to run the offline Noah LSM, and the SMAP soil moisture observation data were assimilated by applying the EnKF data assimilation technique. The soil moisture data obtained from the offline LSM simulation including the data assimilation process were used as the initial data for the WRF model. To investigate the effect of soil moisture initialization, CTL and LIS experiments were conducted using the soil moisture fields from the FNL and LIS for the initial surface conditions of the WRF model, respectively. Compared to the CTL experiment, the LIS experiment simulated drier soil conditions and a more realistic SAT and 500 GPH over Northeast Asia during the 21-day simulation period. In particular, soil moisture initialization had a more notable effect over Mongolia toward the mid-to-end period of the simulation. A positive ΔSAT between the LIS and the CTL experiments prevailed over Mongolia from the start of the model simulation, and the difference became larger as the Δ500 GPH increased. The warmer SAT in the LIS experiment in Week 1 was induced by a lower LHF and the drier soil conditions. Mid-upper atmospheric anticyclonic circulation responded to the soil moisture-induced low-level heat source during Weeks 2 and 3. The anticyclonic anomaly in the mid-to-upper atmosphere became strong and spatially expanded, and the positive ΔSAT increased further. Consequently, we found that the soil moisture initialization by the LIS spin-up improved the simulation performance of the 2016 Northeast Asia heat wave both spatially (Mongolia to Northeast Asia) and temporally (Weeks 1, 2, and 3), resulting in more realistic land–atmosphere interactions and surface fluxes.

With the increasing number of 2016-type heat wave events associated with continental thermal highs over Mongolia (Ha et al., 2022; Yoon et al., 2020; Zhang et al., 2020), this study is meaningful in that it suggests an effective way to improve the simulation performance for these events. Especially, the suggestion that heat wave in the focusing area can continue and become intensified in the future supports the importance of the implications mentioned in this study. For example, Ha et al. (2022) revealed that the intensification of dry heat wave events over northern China and Mongolia was simulated under the future emission scenario of phase six of the Coupled Model Intercomparison Project (see also Figure 6 of Ha et al., 2022).

Since Northeast Asia also experienced extremely hot events in 2018, we applied the same soil moisture initialization process and assessed its impact. In contrast to the 2016 heat wave, SAT during the simulation period (16 July–6 August 2018) had much less significant improvements (1.38 and 1.1°C in CTL and LIS experiments, respectively) than that in 2016 (Figure 9). There can be several reasons for the weak impact of soil moisture initialization in 2018. First, the difference in soil moisture between the LIS and CTL experiments was smaller in 2018 than in 2016 (Figure S2 in Supporting Information S1). Primarily, resulting from further investigation, the difference in circulation background (Su et al., 2014) could be the main reason. The impact of initial soil moisture conditions in 2016 and 2018 was compared by decreasing LIS soil moisture to 50% only over Mongolia

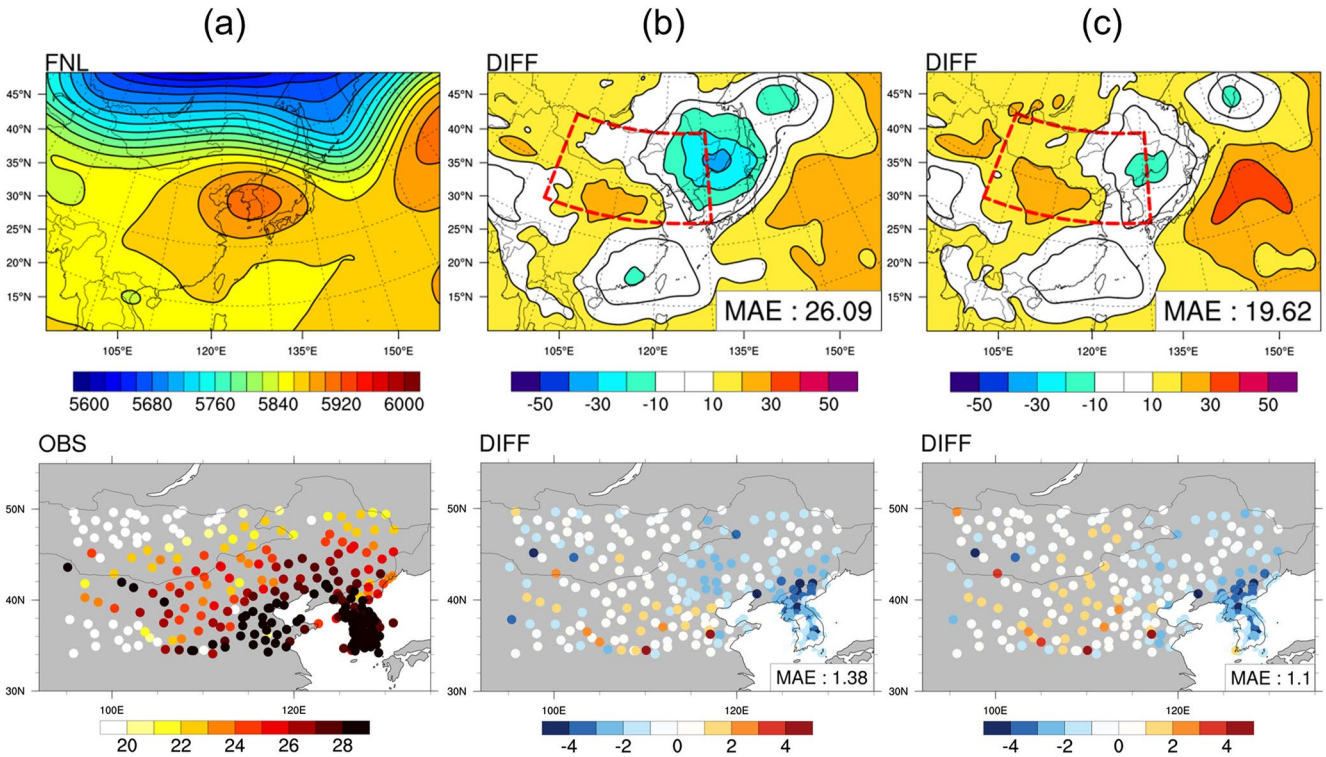

Figure 9. Same as Figure 4 but for a heat wave event in 2018.

(LIS50 experiment; Figures 10a and 10b). As a result, the spatial distribution of differences in SAT and 500 GPH between LIS50 and LIS (ΔSAT_{50} and $\Delta 500\ GPH_{50}$) during the 2016 case has a similar pattern to those of ΔSAT and Δ500 GPH (Figures 10c and 6b), whereas only that of ΔSAT_{50} was comparable and $\Delta 500\ GPH_{50}$ had a negligible value in the 2018 case (Figure 10d). That is, SAT in the 2018 case was responded only by diabatic process (i.e., drier soil moisture and lower LHF-induced warming) of land–atmosphere interaction. This can be the reason for the weaker impact of soil moisture initialization in 2018 than in 2016.

The delayed effect of soil moisture initialization presented in this study can be also related to the circulation background. It is noteworthy that the heat wave event in 2016 over Mongolia was the most intense during Week 3. As represented in Figure 11, the observed (reanalysis) 500 GPH and SAT were maximum in Week 3 when the impact of soil moisture initialization was significant. Moreover, the difference in soil moisture in the initial time was almost maintained during the simulation period in all soil layers (Figure 3 and Figure S1 in Supporting Information S1), although only initial soil moisture condition was replaced in the LIS experiment. Thus, it can be seen that the land–atmosphere interactions were notably amplified in Week 3. Nevertheless, it seems that it takes time to initiate the onset of the land–atmosphere feedback, as reported by a previous study (Zeng et al., 2014). Further analysis is required to unveil the factors for the delay.

The result presents the possibility that the impact of soil moisture initialization can vary according to the different types of heat waves. For example, Lee et al. (2020) revealed that the intensification and expansion of the western North Pacific high affected the 2018 South Korean heat wave, but was weak in 2016. Rather, previous studies emphasized that the 2016 heat wave could have been associated with the positive geopotential anomaly related to the deficit of soil moisture over East Asia (Seo et al., 2020). These distinct synoptic features in both heat wave cases were also observed in this study (Figures 2a and 9a). Yoon et al. (2020) also demonstrated that the 2016 and 2018 heat waves in South Korea could be categorized differently in terms of their synoptic conditions using cluster analysis. In the case of a 2018-type heat wave, other techniques, such as air–sea coupling, might be needed to improve the simulation performance of the numerical weather prediction model (Kim et al., 2020). Nevertheless, further investigation on various heat wave events is required to generalize the impact of soil moisture initialization.

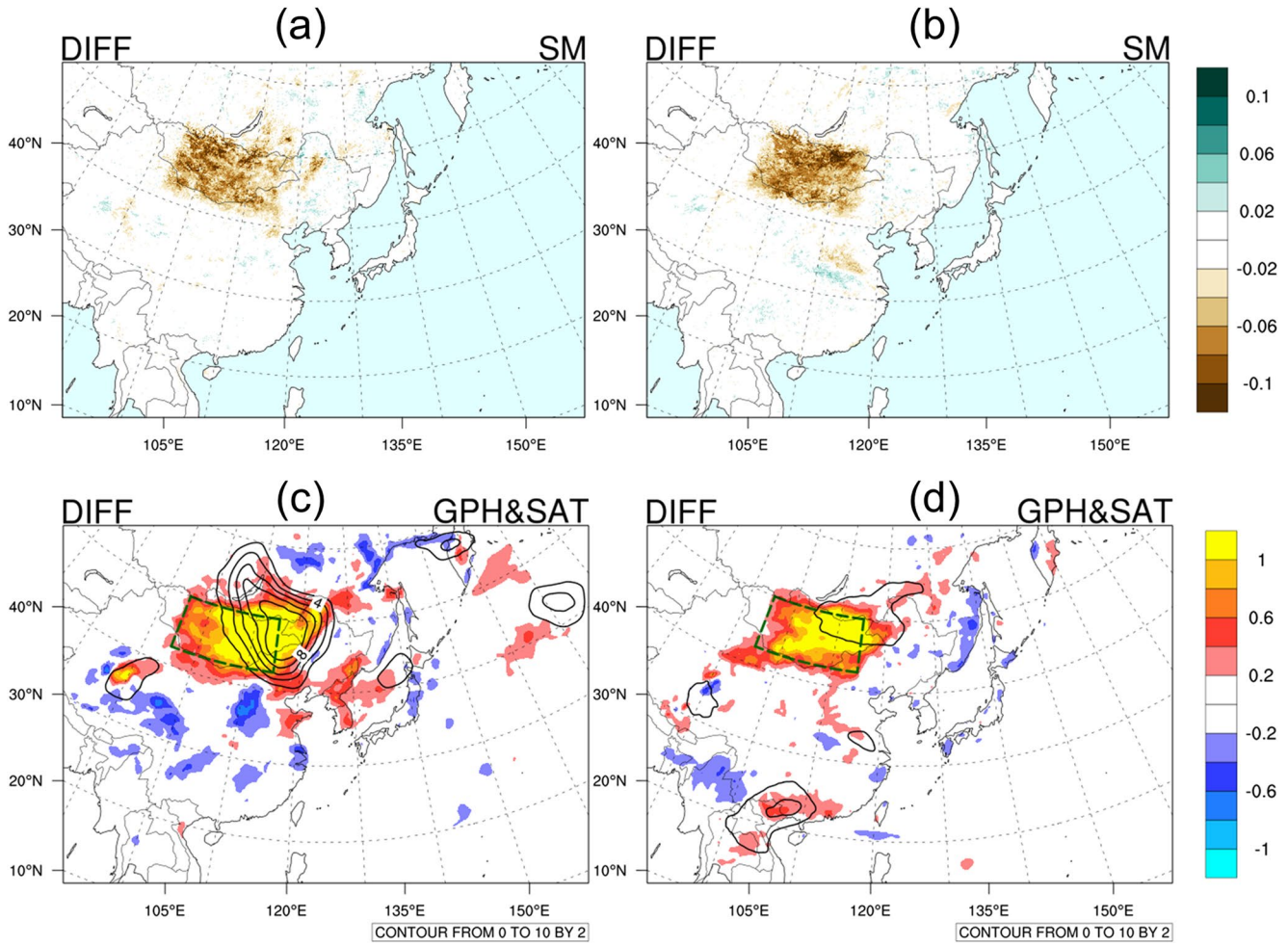

Figure 10. Differences in the (a and b) surface soil moisture content ($m^3\ m^{-3}$), and (c and d) SAT_{50} (°C) (shading) with 500 GPH_{50} (gpm) (contour) between the LIS50 and Land Information System experiments during the simulation period of 2016 (left column) and 2018 (right column).

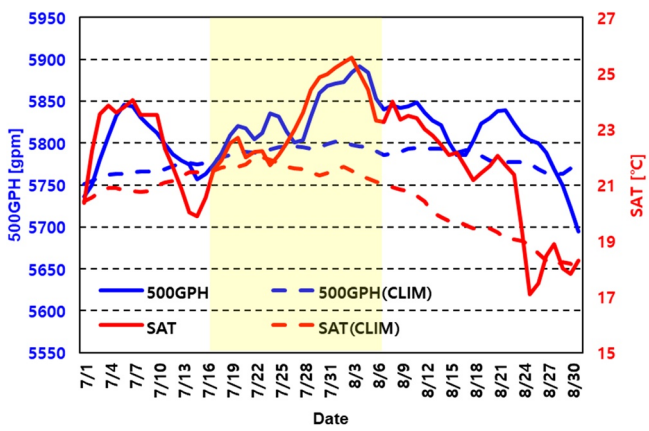

Figure 11. Time series of 500 GPH (blue lines) and surface air temperature (red lines) over Mongolia during July–August 2016. Solid lines indicate each variable in 2016 and dashed lines indicate climatological mean during 1979–2018. Yellow shaded area indicates the simulation period. All results were derived from the European Centre for Medium-Range Weather Forecasts ERA-Interim data (https://rda.ucar.edu/datasets/ds627.0/).

Although many previous studies have examined the added value of soil moisture data assimilation compared to offline LSM simulation (Santanello Jr et al., 2016; E. Seo et al., 2021), the impacts of offline LSM simulation and soil moisture data assimilation were not distinguished in this study. Therefore, comparisons of soil moisture initialization impacts using soil moisture data (a) with and without data assimilation (i.e., soil moisture data assimilation vs. offline LSM) and (b) assimilated from various satellite retrievals (e.g., the Advanced Scatterometer [ASCAT] or the Soil Moisture Operational Product System) remain to be further studied. Moreover, direct evaluation of soil moisture data assimilation products was not carried out because of the lack of in-situ station data over Mongolia. Although further analysis presented a better estimation of soil moisture in South Korea and North America in LIS than FNL (not shown), a direct evaluation of soil moisture for the study region (i.e., East Asia and Mongolia) is desired. Lastly, we did a one-day-lagged simulation (e.g., simulation started from 15 to 17 July) to perturb the initial state and got qualitatively similar results (not shown). However, an ensemble simulation by randomly permuting initial conditions, especially strongly associated with the land–atmosphere interaction (e.g., atmospheric boundary layer winds) (Wei et al., 2021) is required to establish the reliability of the simulation result.

Data Availability Statement

The Weather Research and Forecasting (WRF) model is available at https://www2.mmm.ucar.edu [Software] (WRF, 2008). Figures have been made with the National Center for Atmospheric Research (NCAR) Command Language (NCL) post-processing tool accessible at https://www.ncl.ucar.edu [Software] (NCL, 2019). The meteorological input data to create the initial and boundary conditions for the WRF model domains were obtained from the Global Forecast System (GFS) forecast and analysis data available at the National Centers for Environmental Information (NCEI) online at http://ncei.noaa.gov [Dataset] (GFS, 2015). The WRF simulation data can be accessed on the GitHub repository (https://doi.org/10.5281/zenodo.7033943) (Yoon & Cha, 2022). ERA5 hourly data on pressure levels were provided by ECMWF (ERA5, 2018). ERA-Interim hourly data on pressure levels were provided by ECMWF (ERA-Interim, 2009).

Acknowledgments
This work was funded by the Korea Meteorological Administration Research and Development Program under Grant KMIPA 2017-7010, and supported by Korea Environment Industry & Technology Institute (KEITI) through "Climate Change R&D Project for New Climate Regime", funded by Korea Ministry of Environment (MOE) 2022003560002.

References

Azhar, G. S., Mavalankar, D., Nori-Sarma, A., Rajiva, A., Dutta, P., Jaiswal, A., et al. (2014). Heat-related mortality in India: Excess all-cause mortality associated with the 2010 Ahmedabad heat wave. *PLoS One*, *9*(3), e91831. https://doi.org/10.1371/journal.pone.0091831

Chen, F., Manning, K. W., LeMone, M. A., Trier, S. B., Alfieri, J. G., Roberts, R., et al. (2007). Description and evaluation of the characteristics of the NCAR high-resolution land data assimilation system. *Journal of Applied Meteorology and Climatology*, *46*(6), 694–713. https://doi.org/10.1175/jam2463.1

Chen, F., Mitchell, K., Schaake, J., Xue, Y., Pan, H. L., Koren, V., et al. (1996). Modeling of land surface evaporation by four schemes and comparison with FIFE observations. *Journal of Geophysical Research*, *101*(D3), 7251–7268. https://doi.org/10.1029/95jd02165

Chun, J. A., Lee, E., Kim, D., Kim, S. T., & Lee, W.-S. (2020). Evaluation of near-realtime weekly root-zone soil moisture index (SMI) for the extreme climate monitoring web-service across East Asia (in Korean). *Journal of Korea Water Resources Association*, *53*(6), 409–416.

Cosgrove, B. A., Lohmann, D., Mitchell, K. E., Houser, P. R., Wood, E. F., Schaake, J. C., et al. (2003). Land surface model spin-up behavior in the North American land data assimilation system (NLDAS). *Journal of Geophysical Research*, *108*(D22), 8845. https://doi.org/10.1029/2002jd003316

Coumou, D., Robinson, A., & Rahmstorf, S. (2013). Global increase in record-breaking monthly-mean temperatures. *Climatic Change*, *118*(3–4), 771–782. https://doi.org/10.1007/s10584-012-0668-1

Deng, K., Yang, S., Ting, M., Zhao, P., & Wang, Z. (2019). Dominant modes of China summer heat waves driven by global sea surface temperature and atmospheric internal variability. *Journal of Climate*, *32*(12), 3761–3775. https://doi.org/10.1175/jcli-d-18-0256.1

Dirmeyer, P. A., Balsamo, G., Blyth, E. M., Morrison, R., & Cooper, H. M. (2021). Land-atmosphere interactions exacerbated the drought and heatwave over northern Europe during summer 2018. *AGU Advances*, *2*(2), e2020AV000283. https://doi.org/10.1029/2020av000283

Dirmeyer, P. A., Wu, J., Norton, H. E., Dorigo, W. A., Quiring, S. M., Ford, T. W., et al. (2016). Confronting weather and climate models with observational data from soil moisture networks over the United States. *Journal of Hydrometeorology*, *17*(4), 1049–1067. https://doi.org/10.1175/jhm-d-15-0196.1

Draper, C., Reichle, R., De Lannoy, G., & Liu, Q. (2012). Assimilation of passive and active microwave soil moisture retrievals. *Geophysical Research Letters*, *39*(4), L04401. https://doi.org/10.1029/2011gl050655

Dudhia, J. (1989). Numerical study of convection observed during the winter monsoon experiment using a mesoscale two-dimensional model. *Journal of the Atmospheric Sciences*, *46*(20), 3077–3107. https://doi.org/10.1175/1520-0469(1989)046<3077:nsocod>2.0.co;2

Dunn, R. J., Willett, K. M., Parker, D. E., & Mitchell, L. (2016). Expanding HadISD: Quality-controlled, sub-daily station data from 1931. *Geoscientific Instrumentation, Methods and Data Systems*, *5*(2), 473–491. https://doi.org/10.5194/gi-5-473-2016

ERA5. (2018). ERA5 hourly data on pressure levels from 1959 to present [Dataset]. Copernicus/ECMWF. Retrieved from https://cds.climate.copernicus.eu/cdsapp#!/dataset/reanalysis-era5-pressure-levels

ERA-Interim. (2009). ERA-interim project [Dataset]. Interim. https://doi.org/10.5065/D6CR5RD9

Erdenebat, E., & Sato, T. (2016). Recent increase in heat wave frequency around Mongolia: Role of atmospheric forcing and possible influence of soil moisture deficit. *Atmospheric Science Letters*, *17*(2), 135–140. https://doi.org/10.1002/asl.616

Erdenebat, E., & Sato, T. (2018). Role of soil moisture-atmosphere feedback during high temperature events in 2002 over Northeast Eurasia. *Progress in Earth and Planetary Science*, *5*(1), 37. https://doi.org/10.1186/s40645-018-0195-4

Fischer, E. M., Seneviratne, S. I., Vidale, P. L., Lüthi, D., & Schär, C. (2007). Soil moisture-atmosphere interactions during the 2003 European summer heat wave. *Journal of Climate*, *20*(20), 5081–5099. https://doi.org/10.1175/jcli4288.1

GFS. (2015). NCEP GDAS/FNL 0.25 degree global tropospheric analyses and forecast grids [Dataset]. GFS. Retrieved from https://rda.ucar.edu/datasets/ds083.3/index.html%23%21description

Ha, K. J., Seo, Y. W., Yeo, J. H., Timmermann, A., Chung, E. S., Franzke, C. L., et al. (2022). Dynamics and characteristics of dry and moist heatwaves over East Asia. *npj Climate and Atmospheric Science*, *5*(1), 1–11. https://doi.org/10.1038/s41612-022-00272-4

Han, J., & Pan, H. L. (2011). Revision of convection and vertical diffusion schemes in the NCEP Global Forecast System. *Weather and Forecasting*, *26*(4), 520–533. https://doi.org/10.1175/waf-d-10-05038.1

Hong, S.-Y., & Lim, J.-O. J. (2006). The WRF single-moment 6-class microphysics scheme (WSM6). *Asia-Pacific Journal of Atmospheric Sciences*, *42*(2), 129–151.

Hong, S.-Y., Noh, Y., & Dudhia, J. (2006). A new vertical diffusion package with an explicit treatment of entrainment processes. *Monthly Weather Review*, *134*(9), 2318–2341. https://doi.org/10.1175/mwr3199.1

Hu, F., Wei, Z., Yang, X., Xie, W., Li, Y., Cui, C., et al. (2022). Assessment of SMAP and SMOS soil moisture products using triple collocation method over inner Mongolia. *Journal of Hydrology: Regional Studies*, *40*, 101027. https://doi.org/10.1016/j.ejrh.2022.101027

Huffman, G. J., Bolvin, D. T., Braithwaite, D., Hsu, K., Joyce, R., Xie, P., & Yoo, S.-H. (2015). NASA global precipitation measurement (GPM) integrated multi-satellite retrievals for GPM (IMERG). *Algorithm Theoretical Basis Document (ATBD) Version*, *4*, 26.

Huffman, G. J., Bolvin, D. T., Nelkin, E. J., & Tan, J. J. N. G. C. (2015). Integrated Multi-satellitE Retrievals for GPM (IMERG) technical documentation. *NASA/GSFC Code*, *612*(47), 2019.

Imada, Y., Watanabe, M., Kawase, H., Shiogama, H., & Arai, M. (2019). The July 2018 high temperature event in Japan could not have happened without human-induced global warming. *Sola*, *15A*. https://doi.org/10.2151/sola.15A-002

Jun, S., Park, J.-H., Choi, H.-J., Lee, Y.-H., Lim, Y.-J., Boo, K.-O., & Kang, H.-S. (2021). Impact of soil moisture data assimilation on analysis and medium-range forecasts in an operational global data assimilation and prediction system. *Atmosphere*, *12*(9), 1089. https://doi.org/10.3390/atmos12091089

Kim, E.-J., Marzin, C., Milton, S. F., Boo, K.-O., Kim, Y., Oh, J., & Kang, H.-S. (2020). Representation of the 2016 Korean heatwave in the unified model global NWP forecasts: The impact of remotely forced model errors and atmosphere-ocean coupling. *Atmosphere*, *11*(12), 1275. https://doi.org/10.3390/atmos11121275

Knowlton, K., Rotkin-Ellman, M., King, G., Margolis, H. G., Smith, D., Solomon, G., et al. (2009). The 2006 California heat wave: Impacts on hospitalizations and emergency department visits. *Environmental Health Perspectives*, *117*(1), 61–67. https://doi.org/10.1289/ehp.11594

Koren, V., Schaake, J., Mitchell, K., Duan, Q. Y., Chen, F., & Baker, J. (1999). A parameterization of snowpack and frozen ground intended for NCEP weather and climate models. *Journal of Geophysical Research*, *104*(D16), 19569–19585. https://doi.org/10.1029/1999jd900232

Koster, R. D., & Suarez, M. J. (2003). Impact of land surface initialization on seasonal precipitation and temperature prediction. *Journal of Hydrometeorology*, *4*(2), 408–423. https://doi.org/10.1175/1525-7541(2003)4<408:iolsio>2.0.co;2

Kumar, S. V., Jasinski, M., Mocko, D. M., Rodell, M., Borak, J., Li, B., et al. (2019). NCA-LDAS land analysis: Development and performance of a multisensor, multivariate land data assimilation system for the national climate assessment. *Journal of Hydrometeorology*, *20*(8), 1571–1593. https://doi.org/10.1175/jhm-d-17-0125.1

Kumar, S. V., Peters-Lidard, C. D., Tian, Y., Houser, P. R., Geiger, J., Olden, S., et al. (2006). Land information system: An interoperable framework for high resolution land surface modeling. *Environmental Modelling & Software*, *21*(10), 1402–1415. https://doi.org/10.1016/j.envsoft.2005.07.004

Kumar, S. V., Reichle, R. H., Harrison, K. W., Peters-Lidard, C. D., Yatheendradas, S., & Santanello, J. A. (2012). A comparison of methods for a priori bias correction in soil moisture data assimilation. *Water Resources Research*, *48*(3), W03515. https://doi.org/10.1029/2010wr010261

Kumar, S. V., Reichle, R. H., Peters-Lidard, C. D., Koster, R. D., Zhan, X., Crow, W. T., et al. (2008). A land surface data assimilation framework using the land information system: Description and applications. *Advances in Water Resources*, *31*(11), 1419–1432. https://doi.org/10.1016/j.advwatres.2008.01.013

Lee, H.-D., Min, K.-H., Bae, J.-H., & Cha, D.-H. (2020). Characteristics and comparison of 2016 and 2018 heat wave in Korea (in Korean). *Atmosphere*, *30*(1), 1–15.

Li, Y., Ren, G., You, Q., Wang, Q., Niu, Q., & Mu, L. (2022). The 2016 record-breaking marine heatwave in the Yellow Sea and associated atmospheric circulation anomalies. *Atmospheric Research*, *268*. 106011. https://doi.org/10.1016/j.atmosres.2021.106011

Lim, Y.-J., Byun, K.-Y., Lee, T.-Y., Kwon, H., Hong, J., & Kim, J. (2012). A land data assimilation system using the MODIS-derived land data and its application to numerical weather prediction in East Asia. *Asia-Pacific Journal of Atmospheric Sciences*, *48*(1), 83–95. https://doi.org/10.1007/s13143-012-0008-4

Lim, Y.-J., Hong, J., & Lee, T.-Y. (2012). Spin-up behavior of soil moisture content over East Asia in a land surface model. *Meteorology and Atmospheric Physics*, *118*(3), 151–161. https://doi.org/10.1007/s00703-012-0212-x

Lin, P., Wei, J., Yang, Z.-L., Zhang, Y., & Zhang, K. (2016). Snow data assimilation-constrained land initializations improve seasonal temperature predictions. *Geophysical Research Letters*, *43*(21), 11423–11432. https://doi.org/10.1002/2016GL070966

Lin, P., Yang, Z.-L., Wei, J., Dickinson, R. E., Zhang, Y., & Zhao, L. (2020). Assimilating multi-satellite snow data in ungauged Eurasia improves the simulation accuracy of Asian monsoon seasonal anomalies. *Environmental Research Letters*, *15*(6), 064033. https://doi.org/10.1088/1748-9326/ab80ef

Lin, T. S., & Cheng, F. Y. (2016). Impact of soil moisture initialization and soil texture on simulated land-atmosphere interaction in Taiwan. *Journal of Hydrometeorology*, *17*(5), 1337–1355. https://doi.org/10.1175/jhm-d-15-0024.1

Lorenz, R., Jaeger, E. B., & Seneviratne, S. I. (2010). Persistence of heat waves and its link to soil moisture memory. *Geophysical Research Letters*, *37*(9), L09703. https://doi.org/10.1029/2010gl042764

Lu, Y., Steele-Dunne, S. C., Farhadi, L., & van de Giesen, N. (2017). Mapping surface heat fluxes by assimilating SMAP soil moisture and GOES land surface temperature data. *Water Resources Research*, *53*(12), 10858–10877. https://doi.org/10.1002/2017wr021415

Martius, O., Wehrli, K., & Rohrer, M. (2021). Local and remote atmospheric responses to soil moisture anomalies in Australia. *Journal of Climate*, *34*(22), 9115–9131. https://doi.org/10.1175/jcli-d-21-0130.1

Meehl, G. A., & Tebaldi, C. (2004). More intense, more frequent, and longer lasting heat waves in the 21st century. *Science*, *305*(5686), 994–997. https://doi.org/10.1126/science.1098704

Min, K. H., Chung, C. H., Bae, J. H., & Cha, D. H. (2020). Synoptic characteristics of extreme heatwaves over the Korean Peninsula based on ERA Interim reanalysis data. *International Journal of Climatology*, *40*(6), 3179–3195. https://doi.org/10.1002/joc.6390

Miralles, D. G., Gentine, P., Seneviratne, S. I., & Teuling, A. J. (2019). Land-atmospheric feedbacks during droughts and heatwaves: State of the science and current challenges. *Annals of the New York Academy of Sciences*, *1436*(1), 19–35. https://doi.org/10.1111/nyas.13912

Miralles, D. G., Teuling, A. J., Van Heerwaarden, C. C., & Vilà-Guerau de Arellano, J. (2014). Mega-heatwave temperatures due to combined soil desiccation and atmospheric heat accumulation. *Nature Geoscience*, *7*(5), 345–349. https://doi.org/10.1038/ngeo2141

Miralles, D. G., Van Den Berg, M., Teuling, A., & De Jeu, R. (2012). Soil moisture-temperature coupling: A multiscale observational analysis. *Geophysical Research Letters*, *39*(21), L21707. https://doi.org/10.1029/2012gl053703

NCL. (2019). The NCAR Command Language [Software]. NCL. https://doi.org/10.5065/D6WD3XH5

O'Neill, P. E., Chan, S., Njoku, E. G., Jackson, T., Bindlish, R., & Chaubell, J. (2021). *SMAP L3 radiometer global daily 36 km EASE-grid soil moisture, version 8*. NASA National Snow and Ice Data Center Distributed Active Archive Center. https://doi.org/10.5067/OMHVSRGFX38O

Poumadere, M., Mays, C., Le Mer, S., & Blong, R. (2005). The 2003 heat wave in France: Dangerous climate change here and now. *Risk Analysis: International Journal*, *25*(6), 1483–1494. https://doi.org/10.1111/j.1539-6924.2005.00694.x

Prodhomme, C., Doblas-Reyes, F., Bellprat, O., & Dutra, E. (2016). Impact of land-surface initialization on sub-seasonal to seasonal forecasts over Europe. *Climate Dynamics*, *47*(3), 919–935. https://doi.org/10.1007/s00382-015-2879-4

Quesada, B., Vautard, R., Yiou, P., Hirschi, M., & Seneviratne, S. I. (2012). Asymmetric European summer heat predictability from wet and dry southern winters and springs. *Nature Climate Change*, *2*(10), 736–741. https://doi.org/10.1038/nclimate1536

Reichle, R. H., Crow, W. T., & Keppenne, C. L. (2008). An adaptive ensemble Kalman filter for soil moisture data assimilation. *Water Resources Research*, *44*(3), W03423. https://doi.org/10.1029/2007wr006357

Reichle, R. H., De Lannoy, G. J., Liu, Q., Ardizzone, J. V., Colliander, A., Conaty, A., et al. (2017). Assessment of the SMAP level-4 surface and root-zone soil moisture product using in situ measurements. *Journal of Hydrometeorology*, *18*(10), 2621–2645. https://doi.org/10.1175/jhm-d-17-0063.1

Reichle, R. H., & Koster, R. D. (2004). Bias reduction in short records of satellite soil moisture. *Geophysical Research Letters*, *31*(19), L19501. https://doi.org/10.1029/2004gl020938

Reichle, R. H., McLaughlin, D. B., & Entekhabi, D. (2002). Hydrologic data assimilation with the ensemble Kalman filter. *Monthly Weather Review*, *130*(1), 103–114. https://doi.org/10.1175/1520-0493(2002)130<0103:hdawte>2.0.co;2

Ren, L., Zhou, T., & Zhang, W. (2020). Attribution of the record-breaking heat event over Northeast Asia in summer 2018: The role of circulation. *Environmental Research Letters*, *15*(5), 054018. https://doi.org/10.1088/1748-9326/ab8032

Rodell, M., Houser, P., Berg, A., & Famiglietti, J. (2005). Evaluation of 10 methods for initializing a land surface model. *Journal of Hydrometeorology*, *6*(2), 146–155. https://doi.org/10.1175/jhm414.1

Rodell, M., Houser, P., Jambor, U., Gottschalck, J., Mitchell, K., Meng, C.-J., et al. (2004). The global land data assimilation system. *Bulletin of the American Meteorological Society*, *85*(3), 381–394. https://doi.org/10.1175/bams-85-3-381

Santanello, J. A., Jr., Kumar, S. V., Peters-Lidard, C. D., & Lawston, P. M. (2016). Impact of soil moisture assimilation on land surface model spinup and coupled land-atmosphere prediction. *Journal of Hydrometeorology*, *17*(2), 517–540. https://doi.org/10.1175/jhm-d-15-0072.1

Schumacher, D. L., Keune, J., Dirmeyer, P., & Miralles, D. G. (2022). Drought self-propagation in drylands due to land–atmosphere feedbacks. *Nature Geoscience*, *15*(4), 262–268. https://doi.org/10.1038/s41561-022-00912-7

Seneviratne, S. I., Corti, T., Davin, E. L., Hirschi, M., Jaeger, E. B., Lehner, I., et al. (2010). Investigating soil moisture–climate interactions in a changing climate: A review. *Earth-Science Reviews*, *99*(3–4), 125–161. https://doi.org/10.1016/j.earscirev.2010.02.004

Seneviratne, S. I., Lüthi, D., Litschi, M., & Schär, C. (2006). Land-atmosphere coupling and climate change in Europe. *Nature*, *443*(7108), 205–209. https://doi.org/10.1038/nature05095

Seo, E., & Dirmeyer, P. A. (2022). Understanding the diurnal cycle of land-atmosphere interactions from flux site observations. *Hydrology and Earth System Sciences*, *26*(20), 5411–5429. https://doi.org/10.5194/hess-26-5411-2022

Seo, E., Lee, M.-I., Jeong, J.-H., Koster, R. D., Schubert, S. D., Kim, H.-M., et al. (2019). Impact of soil moisture initialization on boreal summer subseasonal forecasts: Mid-latitude surface air temperature and heat wave events. *Climate Dynamics*, *52*(3–4), 1695–1709. https://doi.org/10.1007/s00382-018-4221-4

Seo, E., Lee, M.-I., & Reichle, R. H. (2021). Assimilation of SMAP and ASCAT soil moisture retrievals into the JULES land surface model using the Local Ensemble Transform Kalman Filter. *Remote Sensing of Environment*, *253*, 112222. https://doi.org/10.1016/j.rse.2020.112222

Seo, E., Lee, M. I., Schubert, S. D., Koster, R. D., & Kang, H. S. (2020). Investigation of the 2016 Eurasia heat wave as an event of the recent warming. *Environmental Research Letters*, *15*(11), 114018. https://doi.org/10.1088/1748-9326/abbbae

Seo, Y.-W., Ha, K.-J., & Park, T.-W. (2021). Feedback attribution to dry heatwaves over East Asia. *Environmental Research Letters*, *16*(6), 064003. https://doi.org/10.1088/1748-9326/abf18f

Skamarock, W. C., Klemp, J. B., Dudhia, J., Gill, D. O., Barker, D. M., Wang, W., & Powers, J. G. (2005). *A description of the advanced research WRF version 2Rep*. National Center For Atmospheric Research Boulder Co Mesoscale and Microscale.

Su, H., Yang, Z. L., Dickinson, R. E., & Wei, J. (2014). Spring soil moisture-precipitation feedback in the Southern Great Plains: How is it related to large-scale atmospheric conditions? *Geophysical Research Letters*, *41*(4), 1283–1289. https://doi.org/10.1002/2013gl058931

Tangdamrongsub, N., Han, S.-C., Yeo, I.-Y., Dong, J., Steele-Dunne, S. C., Willgoose, G., & Walker, J. P. (2020). Multivariate data assimilation of GRACE, SMOS, SMAP measurements for improved regional soil moisture and groundwater storage estimates. *Advances in Water Resources*, *135*, 103477. https://doi.org/10.1016/j.advwatres.2019.103477

van den Hurk, B., Doblas-Reyes, F., Balsamo, G., Koster, R. D., Seneviratne, S. I., & Camargo, H. (2012). Soil moisture effects on seasonal temperature and precipitation forecast scores in Europe. *Climate Dynamics*, *38*(1), 349–362. https://doi.org/10.1007/s00382-010-0956-2

Wang, P., Zhang, Q., Yang, Y., & Tang, J. (2019). The sensitivity to initial soil moisture for three severe cases of heat waves over Eastern China. *Frontiers in Environmental Science*, *7*, 18. https://doi.org/10.3389/fenvs.2019.00018

Wei, J., Liu, Y., & Chen, H. (2021). Contrasting responses of local climate to the perturbation of atmospheric boundary layer winds linked to land-atmosphere interactions. *Journal of Geophysical Research: Atmospheres*, *126*(15), e2020JD034508. https://doi.org/10.1029/2020JD034508

WRF. (2008). A description of the advanced Research WRF version 3 [Software]. WRF. Retrieved from https://www2.mmm.ucar.edu/wrf/users/download/get_source.html

Xia, Y., Mitchell, K., Ek, M., Sheffield, J., Cosgrove, B., Wood, E., et al. (2012). Continental-scale water and energy flux analysis and validation for the North American land data assimilation system project phase 2 (NLDAS-2): 1. Intercomparison and application of model products. *Journal of Geophysical Research*, *117*(D3), D03109. https://doi.org/10.1029/2011jd016048

Yeh, S.-W., Won, Y.-J., Hong, J.-S., Lee, K.-J., Kwon, M., Seo, K.-H., & Ham, Y.-G. (2018). The record-breaking heat wave in 2016 over South Korea and its physical mechanism. *Monthly Weather Review*, *146*(5), 1463–1474. https://doi.org/10.1175/mwr-d-17-0205.1

Yoon, D., & Cha, D.-H. (2022). WRF dataset for soil moisture initialization experiments (Final version) [Dataset]. Zenodo. https://doi.org/10.5281/zenodo.7033943

Yoon, D., Cha, D. H., Lee, G., Park, C., Lee, M. I., & Min, K. H. (2018). Impacts of synoptic and local factors on heat wave events over southeastern region of Korea in 2015. *Journal of Geophysical Research: Atmospheres*, *123*(21), 12081–012096. https://doi.org/10.1029/2018jd029247

Yoon, D., Cha, D.-H., Lee, M.-I., Min, K.-H., Jun, S.-Y., & Choi, Y. (2021). Comparison of regional climate model performances for different types of heat waves over South Korea. *Journal of Climate*, *34*(6), 2157–2174. https://doi.org/10.1175/jcli-d-20-0422.1

Yoon, D., Cha, D.-H., Lee, M.-I., Min, K.-H., Kim, J., Jun, S.-Y., & Choi, Y. (2020). Recent changes in heatwave characteristics over Korea. *Climate Dynamics*, *55*(7–8), 1685–1696. https://doi.org/10.1007/s00382-020-05420-1

Zeng, X.-M., Wang, B., Zhang, Y., Song, S., Huang, X., Zheng, Y., et al. (2014). Sensitivity of high-temperature weather to initial soil moisture: A case study using the WRF model. *Atmospheric Chemistry and Physics*, *14*(18), 9623–9639. https://doi.org/10.5194/acp-14-9623-2014

Zhang, H., & Frederiksen, C. (2003). Local and nonlocal impacts of soil moisture initialization on AGCM seasonal forecasts: A model sensitivity study. *Journal of Climate*, *16*(13), 2117–2137. https://doi.org/10.1175/1520-0442(2003)16<2117:lanios>2.0.co;2

Zhang, P., Jeong, J.-H., Yoon, J.-H., Kim, H., Wang, S.-Y. S., Linderholm, H. W., et al. (2020). Abrupt shift to hotter and drier climate over inner East Asia beyond the tipping point. *Science*, *370*(6520), 1095–1099. https://doi.org/10.1126/science.abb3368